IEEE Access
Multidisciplinary ⋮ Rapid Review ⋮ Open Access Journal

Received 26 June 2023, accepted 28 July 2023, date of publication 8 August 2023, date of current version 14 August 2023.

Digital Object Identifier 10.1109/ACCESS.2023.3302523

RESEARCH ARTICLE

Photogeneration and Performance Optimization (PhPO): A New Algorithm to Improve the Performance of Vertical Epitaxial Hetero-Structure Architecture Laser Power Converters

JAVIER F. LOZANO[1], NATALIA SEOANE[1], ENRIQUE COMESAÑA[2], (Member, IEEE), FLORENCIA M. ALMONACID[3], EDUARDO F. FERNÁNDEZ[3], AND ANTONIO GARCÍA-LOUREIRO[1], (Member, IEEE)

[1]Centro Singular de Investigación en Tecnoloxías Intelixentes (CiTiUS), Departamento de Electrónica e Computación, University of Santiago de Compostela, 15782 Santiago de Compostela, Spain
[2]Escola Politécnica Superior de Enxeñaría, Campus Terra, University of Santiago de Compostela, 27002 Lugo, Spain
[3]Advances in Photovoltaic Technology (AdPVTech), CEACTEMA, University of Jaén, 23071 Jaén, Spain

Corresponding author: Javier F. Lozano (javier.fernandez.lozano@rai.usc.es)

This work was supported in part by the Spanish Government, in part by Xunta de Galicia, in part by Junta de Andalucía, and in part by Fondo Europeo de Desarrollo Regional (FEDER) Funds under Grant PID2019-106497RB-I00, Grant P18-RT-1595, Grant PID2019-104834GB-I00, Grant ED431F 2020/008, Grant ED431C 2022/16, Grant RYC-2017-23312, Grant RYC-2017-21910, and Grant PID2022-141623NB-I00.

ABSTRACT The state of the art in the field of high-power laser transmission is dominated by the so called Vertical Epitaxial Hetero-Structure Architecture (VEHSA), which consists of monolithically stacking p/n cells connected by tunnel junctions. This configuration distributes the current between the cells and reduces the losses due to Joule heating. Since assessing the performance of each individual cell is very challenging, the design and optimization of these devices relies on simple approximations based on the Beer-Lambert law, the exponential decay of light, and guessing from published data. The limitations of these approaches are i) the current of each cell may differ from the calculated photocurrent, producing a mismatch and limiting the overall current, ii) the design parameters cannot be individually evaluated, and iii) the loss of accuracy when applied to devices with light trapping mechanisms. In this work, we present a novel optimization methodology aimed to overcome these limitations, based on a meticulous device Technology Computer-Aided Design (TCAD) and an iterative optimization algorithm with two stages: Photogeneration and Performance Optimization (PhPO). The proposed procedure improves the performance of the current state-of-the-art VEHSA devices, allows the use of new semiconductors and makes the design more resilient to a wide range of operation conditions.

INDEX TERMS Device modeling, new algorithm, laser power converters, VEHSA architecture, photo-current optimization, multijunction photovoltaic devices.

I. INTRODUCTION

The high power laser transmission (HPLT) technology has been pointed as a key development in the wireless power transfer (WPT) field [1]. It consists of transmitting power through a monochromatic light to a remote photovoltaic device, or laser power converter (LPC). This technology has the advantage of providing electrical isolation and avoiding electromagnetic interference [2], replacing traditional copper wires when security restrictions require the absence of sparks. Such is the case for workplaces under an ATEX directive, like refineries or mines where there is risk of fire or explosion [3].

The associate editor coordinating the review of this manuscript and approving it for publication was Marcelo Antonio Pavanello.

Dual transmission of power and data [4], [5] and optically powering satellites [6], [7] or aerial vehicles [8], [9] are other possible applications of this technology. Another remarkable aspect is the possibility of deliver power through optic fiber or wireless transmission through free space [3].

Current state-of-the-art LPC devices exceed 60% efficiency values at room temperature [10], [11]. The base materials used are mostly III-V compounds, being GaAs the preferred one [12], since it achieves efficiencies much larger than LPCs based on Si [13] or InGaAsP/InP [14]. Multijunction GaAs LPCs are particularly noteworthy [15], as well as devices with enhanced photon recycling and treatment of thermalization losses [11]. New advances in photovoltaics provide hints for future efficiency improvements, such as new architectures [16], [17], [18], [19] or the use of materials with fewer limitations [20].

The Vertical Epitaxial Hetero-Structure Architecture (VEHSA) stands out among the multijunction LPCs. This arrangement consists of monolithically stacking p/n tunnel junctions [10], which is also the main pathway to achieve ultra-high efficiencies on concentrating photovoltaic solar cells [21]. The major advantage of this architecture is to distribute the current over the p/n junctions, which reduces Joule heating losses. This allows to operate under high laser power concentrations, increasing the efficiency due to the open circuit voltage (V_{oc}) enhancement associated with higher carrier concentration. The V_{oc} also benefits from a greater Fermi level splitting in thin layers [22]. However, the optimization of VEHSA devices is challenging because of the extreme difficulty of evaluating its individual cell currents. Up to date, the optimization is mainly done by simple approximations using the Beer-Lambert law [23], which only accounts for the photogeneration of each cell. This method is only meaningful to VEHSA devices made of well-known direct bandgap materials like GaAs, since design parameters like doping values and relative p/n sizes are extrapolable from published data [24] and the light decays exponentially in the bulk of the device, as no light-trapping mechanisms are needed. Nevertheless, not measuring the currents of each cell hinders the current matching and the optimization of design parameters, reducing the performance of the device. Although new optimizations paths have been described in literature, such as including tabulated quantum efficiency values in the photogenerated current estimation [25], [26], more sophisticated optimization techniques that broaden the range of VEHSAs are missing. This is of particular interest in the context of materials with indirect high-bandgap like silicon carbide, which has been identified as a potential new route to ultra-high efficiency LPCs [27].

In this paper we propose a new universal methodology to optimize the design of VEHSA devices. The procedure, based on combining device modeling with a multistage optimization algorithm, allows not only to further optimize state-of-the-art VEHSAs, but also opens the door to design and optimize new multijunction devices. This feature skips many trial and error processes when manufacturing novel VEHSA devices, considerably reducing costs. This methodology is valid for both direct or indirect bandgap materials, regardless of whether they are powered by laser or by sunlight.

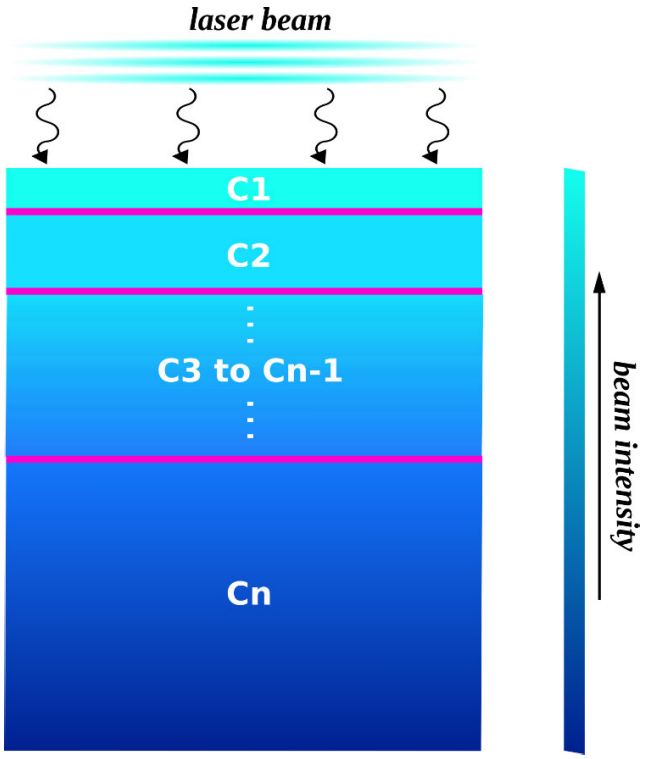

FIGURE 1. Exponential decay of light intensity, according to Beer-Lambert law. To accurately match the photocurrents, the integrated photogeneration must be the same in all cells.

II. METHODOLOGY

In this section we present the main limitations in the design of state-of-the-art VEHSA devices, and we introduce an optimization method to improve their performance via a meticulous current matching and the improvement of the individual efficiency of each cell.

A key factor that affects the performance of VEHSA devices is the precise matching of the currents produced by every cell, since the total current drawn from the device will be the lowest of all the contributing cells. Up to date, the state-of-the-art VEHSAs achieve current matching by applying the Beer-Lambert law, the exponential light decay [23]. The integrated photogeneration must be the same in all cells, as illustrated in **Figure 1:**

$$I_{i+1}(\lambda) = I_i e^{-\alpha(\lambda) t_i} \tag{1}$$

where I_i and I_{i+1} are the light intensities entering and leaving the i-th layer, respectively. t_i is the thickness of the i-th layer and $\alpha(\lambda)$ the wavelength dependent absorption coefficient. This is a good approximation for direct-gap VEHSA devices, as the photogeneration can be calculated very accurately. However, this method does not take into account the performance of each cell, so there will be

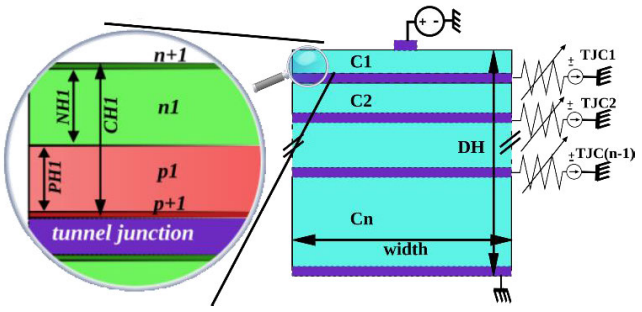

FIGURE 2. 2D-Schematic of a VEHSA device. The variable resistances in tunnel junctions allow to extract the current diferences from the adjacent cells. C1, C2, ..., Cn are the cells of the VEHSA device. The zoom-in shows the detailed structure of the cell C1, composed by n+/n/p/p+ layers, with a CH1 total height. PH1 and NH1 are the heights of C1 p and n layers, respectively.

differences between the photogenerated current and the total current contributed. To avoid this issue, it has been proposed to consider the quantum efficiency, QE, of each cell to calculate the current supplied [25] as follows:

$$I_{abs} = \int \frac{d\boldsymbol{I}_{\boldsymbol{avail}}}{d\boldsymbol{\lambda}} \cdot QE(\boldsymbol{\lambda}) \cdot (\mathbf{1} - \boldsymbol{T}(\boldsymbol{\lambda}) - \boldsymbol{R}(\boldsymbol{\lambda}))d\boldsymbol{\lambda} \quad (2)$$

where I_{abs} and I_{avail} are the absorbed and available photocurrents, R the reflectance, and T the transmittance. This has the advantage of considering beam reflection and transmission, and recombination effects, which are implicit in QE. However, it misses relevant effects such as photon recycling, which is shown to be important in the modeling of GaAs VEHSA devices [28].

These approaches generally provide good results, but the performance worsens as the number of cells increases, due to the current mismatch. The actual record efficiency for a VEHSA at room temperature is achieved by a 5-cell device, reaching a 66.3% [10], and the efficiency consistently decreases for a larger number of cells. Another disadvantage of these approximations is that they are not applicable to indirect bandgap devices that require back texturization for light trapping.

We present an optimization method aimed to overcome these issues valid for both direct or indirect bandgap VEHSAs, independently if they are powered by a laser or by solar light. The system consists of meticulous device TCAD (Technology Computer-Aided Design) of the VEHSA device combined with an iterative optimization algorithm. As modeling tunnel junctions in Silvaco can be problematic [29], we used an standard workaround that consist of modeling the tunnel junctions as perfect conductors [30], to speed-up the simulation time. In these so modeled tunnel junctions we allow the extraction of the tunnel junction currents (TJCs), coupling them to electrodes with lumped variable resistances, as seen in **Figure 2**. These resistances can take very high values to simulate the full device, to avoid current through these contacts, or low realistic values to obtain the differences between the currents produced in adjacent cells. This is a useful tool to accurately match the currents of all cells and improve the performance of the full VEHSA device.

The optimization algorithm is an iterative process involving two stages: Photogeneration and Performance Optimization (PhPO from now on), as shown in **Figure 3**. In the first step, the photogeneration loop, the total device height (DH) is optimized to absorb the largest part of the beam without unnecessarily increasing the size of the device, which will affect the carrier transport. As a first approach the Beer-Lambert law is used to obtain an initial guess. The algorithm iterates, by increasing/decreasing the DH, until two criteria are fulfilled: i) a minimum absorbed light value (photo_low), that establishes the maximum photogeneration losses allowed of the total incident light and ii) a maximum photogeneration value (photo_high), which prevents the device from growing infinitely to absorb the totality of the photons. The resulting optimum DH is then used as an input for the next stage, the performance loop.

In this second stage, the optimizer improves the performance of the cells individually. This process begins with a subroutine that iteratively evaluates the TJCs and modifies *CH1,...*, *CHn*, i.e. the relative sizes of each cell (see Fig' s 2 zoom-in). As the TJCs extracted are the differences between the currents of the adjacent cells, the absolute value represents their mismatch, and the sign of the current indicates which cell is limiting the performance. A negative/positive sign means that the bottom/top cell is limiting and the algorithm modifies the values of *CH1, ...,CHn* to increase the limiting cells in steps normalized by the largest absolute TJC value of all tunnel junctions. This process iterates until all TJCs contribute with the same current and the value is below a certain tolerance, e.g., 1/1000 of the I_{sc} extracted in the anode. When this is achieved, the algorithm optimizes the design parameters, which are the layer relative sizes (*PHi*, *NHi*) and doping values (*PDi*, *NPi*) for every i-th cell, from 1 to n. The optimization algorithm for a single design parameter is described in **Figure 4**. The parameters are swept from an initial value (provided by a preliminary single cell optimization), one by one, with the scope of increasing the cell efficiency. If new optimum design parameters are found, a new iteration is needed, since these optimizations can change the current contributed by each cell and the currents need to be matched again. On the other hand, if during the whole cell optimization cycle no new design parameters are found, the process stops, and it is considered that all cells have achieved their maximum efficiency.

III. RESULTS

To validate our methodology we initially model a GaAs-based 5-cell VEHSA (VEHSA PT5 from now on), that is designed after the experimental device reported by Fafard et al [10], that currently holds the record breaking efficiency at room temperature. We carried the simulation with Silvaco Atlas [31], a device TCAD simulator able to provide realistic and trustable results when modeling a

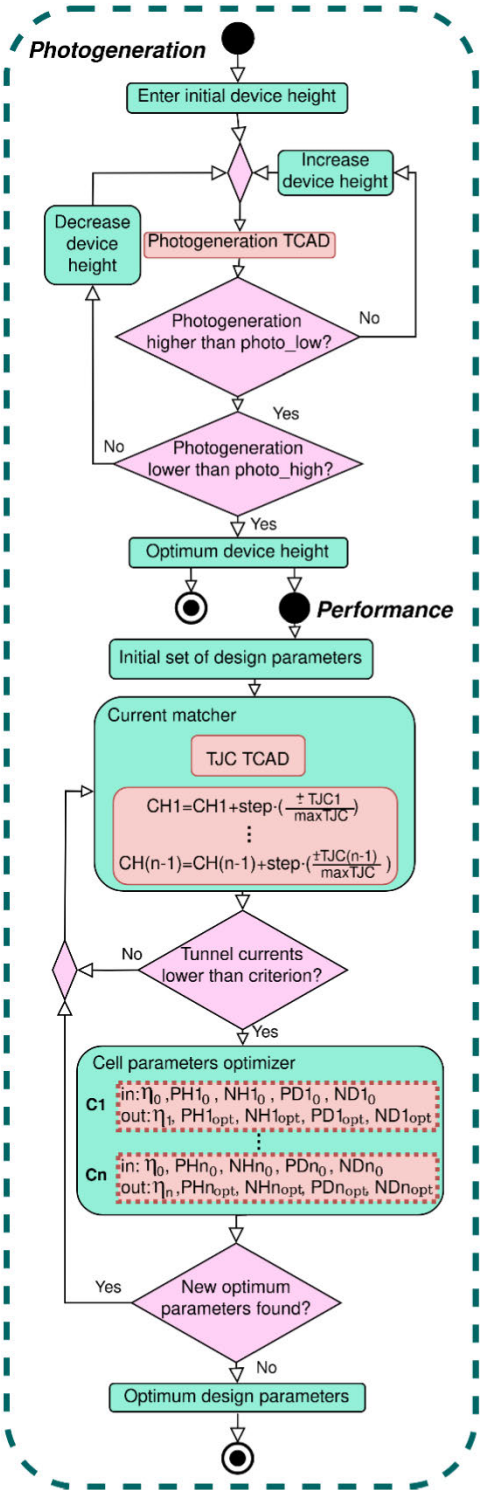

FIGURE 3. Flowchart of the different stages of the PhPO method. Photogeneration TCAD and TJC TCAD are simulations aimed to obtain the photogeneration of each cell and the currents extracted in the tunnel junctions (TJC), respectively. The optimum device height is fixed in the photogeneration loop and used as an input to the performance loop.

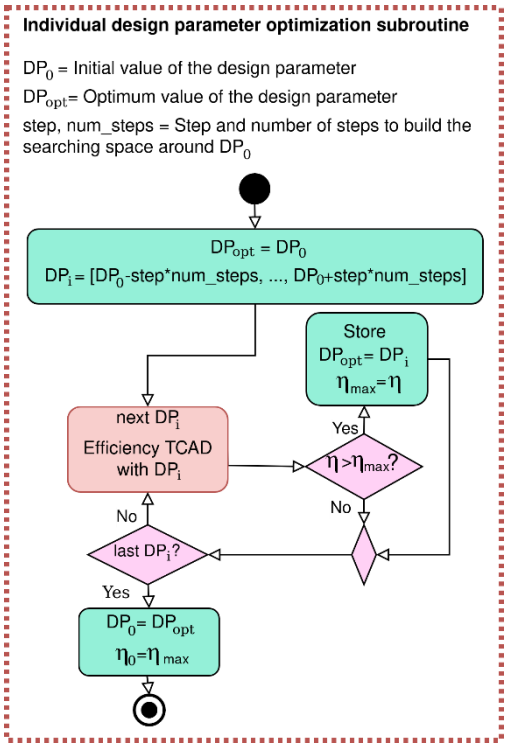

FIGURE 4. Detailed optimization of each design parameter. Efficiency TCAD is the simulation aimed to obtain the efficiency of the evaluated cell. η_0, η, and η_{max} are the initial, latest simulated and maximum efficiencies of the evaluated cell, respectively.

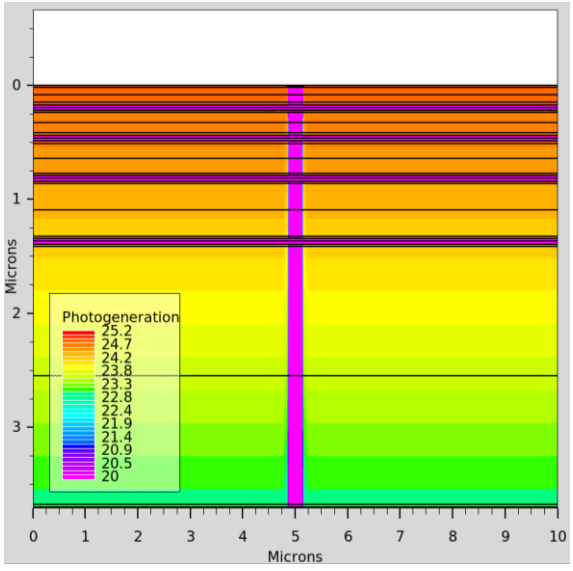

FIGURE 5. Photogeneration rate in a VEHSA PT5.

wide variety of devices, including photovoltaic cells [17], [32]. The Poisson and continuity equations are solved to obtain the characteristics of the device. The beam-device interaction is modelled with the ray tracing method [31] and an example of the photogeneration rate for a VEHSA PT5 is pictured in **Figure 5**. For carrier mobility we use doping concentration-dependent tabulated data, available via Silvaco. The Shockley-Read-Hall (SRH) recombination also considers the doping concentration, following experimental

data [33]. We also include optical and Auger recombinations in the simulation framework. All simulations were performed at T = 298 K. The absorption coefficient used depends on both the doping concentration and the wavelength, and fits experimental curves [34]. The material physical parameters, the incident power and the illumination area are taken from the experimental device supporting information [10]. The width of the device (see Figure 2) is fixed to 10 μm to save computational costs. Since the generation and transport processes occur in the vertical direction and no surface recombination is accounted in this work, which avoids perimeter recombination sources, this decision will not affect the behavior of the device. The contact finger (see Figure 5) covers a 3 percent of the width of the device. Given that no specific design parameters are provided for this particular experimental device, the cell heights (CH) were obtained by applying the Beer-Lambert law [23].

As the light penetrates the device, the CH values increase due to the photogeneration decay in the device, as seen in Figure 1. The CH for each cell includes the n+/n/p/p+ layers as follows: $\mathbf{CH} = \boldsymbol{h_{np+}}\, \boldsymbol{\mathcal{C}}\, \mathbf{h}_{\boldsymbol{np}}$, where h_{np+} is the sum of the p+/n+ layers heights and h_{np} the sum of the n/p layer heights. The p+/n+ layers have fixed heights and doping values of 0.02 μm and $5{\cdot}10^{19}$ cm^{-3}, respectively, selected to accurately match the experimental characteristics. The n/p relative layer heights (NH/PH) are shown as a percent of h_{np} (e.g. n layer height = NH$\cdot$ h_{np}), since this value is fixed by the CH and h_{np+}. The NH/PH values are considered to be equal (0.50/0.50) [10], and the doping values (ND/PD) range from $5{\cdot}10^{17}$-$1.0{\cdot}10^{18}$ cm^{-3}, with thinner cells more heavily doped [25]. The illumination wavelength is fixed to λ =837 nm as in the experimental device. These initial parameters at room temperature are shown in **Table 1**. **Figure 6** shows a comparison between the experimental and the initial calibrated VEHSA PT5 IV curves. Note that in this figure the simulation results are scaled to the illumination area of the experimental device. The device TCAD accurately reproduces the values of I_{sc} and V_{oc} of the experimental device, and the slight differences in the shape of the curve at V_m and intermediate voltages may derive from manufacturing issues.

Once we have demonstrated the validity of our simulation methodology, we apply the PhPO method to further improve the device performance, see in Table 1 the optimized design parameters. The DH slightly increases with respect to the calibration, reaching 3.7 μm. The cell heights have been fine-tuned until the TJC mismatch is below 1/1000 the I_{sc} value of the anode. The relative NH/PH values return much larger n layer heights for thinner cells (e.g., 0.9/0.1 for the first cell), that gradually decrease as the CH increases (e.g., 0.3/0.7 for the fifth cell). The doping values significantly decrease to $1{\cdot}10^{15}$ cm^{-3}, a value three orders of magnitude lower than those observed in the initial design parameters.

The optimized IV curve is also shown in Figure 6 for comparison. The optimized VEHSA PT5 achieves the same V_{oc} as the calibrated and experimental devices and increases the I_{sc} by ≈6%, leading to a 75.8% efficiency, a value 9.5% larger than that of the experimental VEHSA PT5. These improvements are due to the meticulous current matching and individual cell optimization. This can be more clearly seen in **Figure 7** and **Figure 8**, that present the IV curves for each individual cell for the calibrated and optimized devices, respectively. Note that the calibrated VEHSA PT5 individual cell IV curves suffer from current mismatch, and there is also a noticeable V_{oc} mismatch. These effects are drastically reduced in the optimized VEHSA PT5, where the IV curves are very similar for all cells.

Given the wide variety of applications for an LPC, both aerial and terrestrial, it is worthwhile to study the impact of temperature on device performance. For that, the calibrated and optimized VEHSA PT5, are tested at three temperatures:

TABLE 1. Design parameters (DP) for the VEHSA PT5 validation, optimization and constant values. DH and CH are the device and cell heights, NH/PH, N^+/P^+H the n/p, n^+/p^+ layer heights and ND/PD, N^+/P^+D the doping values for the n/p, n^+/p^+ layers, respectively. T is the temperature, λ the incident wavelength and CF the cover factor, which is the portion of the device covered by the contact.

DP	DH [μm]	Cell	CH [μm]	NH [%] / PH [%]	ND [cm^{-3}]	PD [cm^{-3}]
Initial	3.5	1	0.170	0.50/0.50	1e18	1e18
		2	0.218	0.50/0.50	1e18	1e18
		3	0.303	0.50/0.50	1e18	1e18
		4	0.503	0.50/0.50	1e18	1e18
		5	2.306	0.50/0.50	5e17	5e17
Optimized	3.7	1	0.175	0.90/0.10	1e15	1e15
		2	0.227	0.90/0.10	1e15	1e15
		3	0.317	0.60/0.40	1e15	1e15
		4	0.530	0.50/0.50	1e15	1e15
		5	2.450	0.30/0.70	1e15	1e15
Constant	T [K]	Width [μm]	$N^{+/}P^+$H [μm]	$N^{+/}P^+$D [cm^{-3}]	λ [nm]	CF [%]
	298	10	0.02	5e19	837	3

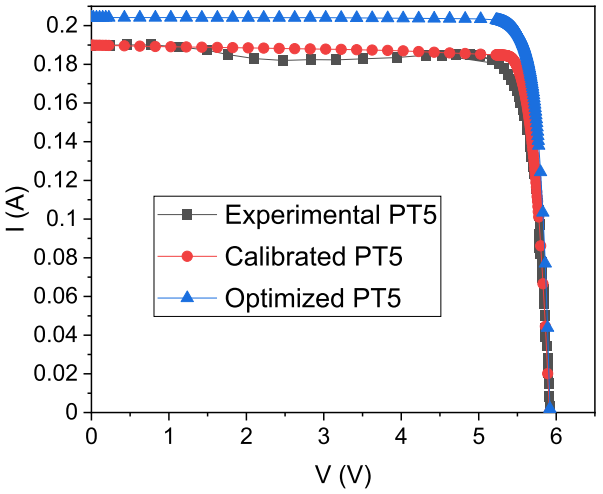

FIGURE 6. IV curves comparing the experimental [12] VEHSA PT5 against the optimized structure provided by the PhPO method. The calibrated VEHSA PT5 is also included as validation.

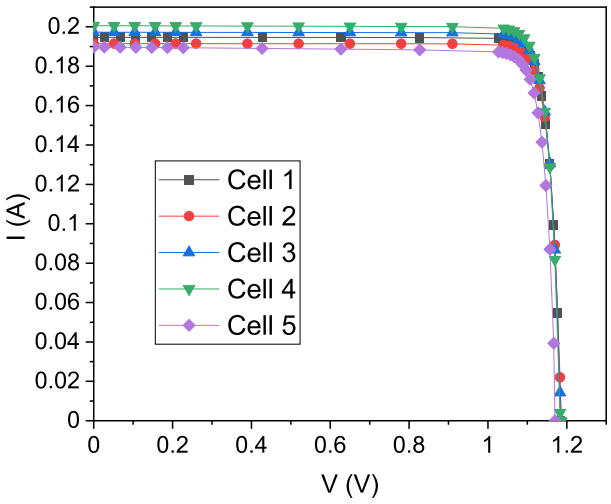

FIGURE 7. IV curves for each cell that composes the calibrated VEHSA PT5. Note that there is an appreciable dispersion in the values of I_{sc} and, to a lesser degree, in those of V_{oc}.

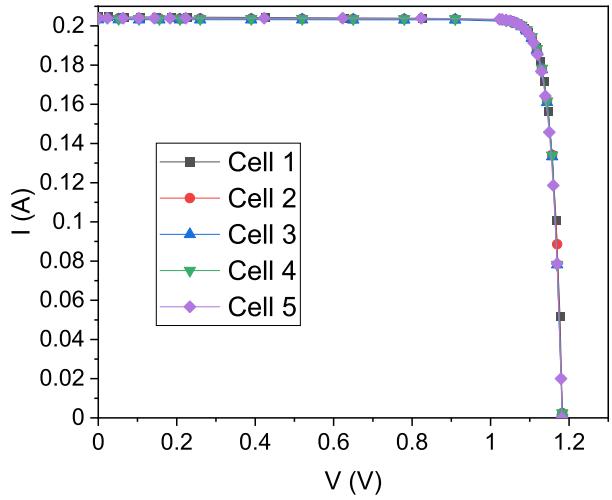

FIGURE 8. IV curves for each cell that composes the optimized VEHSA PT5. Note that, unlike in the case of the calibrated device, there is no dispersion observed in either I_{sc} or V_{oc}.

the standard laboratory conditions (298 K) and ±75 K with respect to this value (223 K and 373 K), in order to evaluate a wide range of operation. The models [35] used in the course of the simulations take into account the dependence on temperature, namely the universal energy bandgap model, SRH concentration-dependent lifetime model, Fermi statistics and power law temperature dependence mobility.

Figure 9 shows the IV curves for the optimized and calibrated VEHSAs PT5 at the three tested temperatures. Note that, although both devices reach the same V_{oc} for each temperature (due to bandgap variation), the optimized VEHSA PT5 achieves the same I_{sc} for all three temperatures tested. This is not the case for the calibrated VEHSA PT5, which suffers from loses in I_{sc} at high temperatures. This is due to the existence of higher recombinations in the experimental device, compared to the optimized one. In the

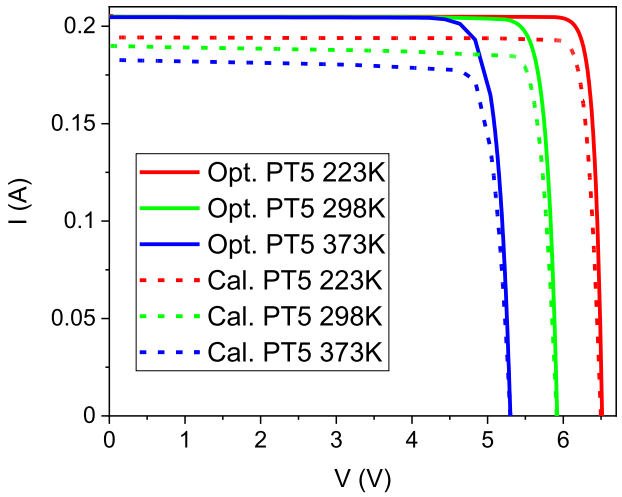

FIGURE 9. IV curves for the optimized (solid lines) and calibrated (dotted lines) VEHSA PT5 at three temperatures: 223 K (blue), 298 K (green) and 373 K (red).

calibrated VEHSA PT5, the efficiency increases/decreases a 11.3% at 223/373 K with respect to the room temperature values. The efficiency of the optimized VEHSA PT5 is slightly less affected by temperature variations, increasing/decreasing a 10.3% at 223/373 K with respect to the room temperature values, respectively. The design parameters obtained through the PhPO method applied at 298 K have considerably reduced the recombinations of the VEHSA PT5, making the device more resilient to a wide range of temperature. Note that, having a single device capable of operating over a broad temperature spectrum without major losses is desirable to avoid the need to manufacture multiple devices.

IV. CONCLUSION

We have presented a new method to optimize the design parameters of VEHSA devices, one of the most efficient architectures of state-of-the-art LPCs. The Photogeneration and Performance Optimization (PhPO) method combines device TCAD with an iterative optimization algorithm. This method is aimed to bypass the main limitations of the VEHSA architecture, namely the current mismatch between cells and the impossibility of tailoring individual cell design parameters. Traditionally, the Beer-Lambert law of exponential decay is the main available tool to match the different cells photogeneration. However, this method obtains low accuracy results when a back reflector or light-trapping mechanisms are included. Another issue related to only applying Beer-Lambert law is that the individual currents of each cell may differ, due to the different performance of the cells, leading to current mismatch.

To validate the PhPO method, we initially modelled the current room temperature record efficiency VEHSA device, a GaAs-based 5-cell reported by Fafard et al. We have accurately reproduced the experimental device IV curves at the same illumination conditions, using similar design parameters. Next, we have applied the iterative optimization algorithm to the calibrated VEHSA. The algorithm has

successfully matched all cells I_{sc} and V_{oc} values and improved each cell performance. This has led to a 9.5% efficiency increase of the optimized device with respect to the experimental VEHSA.

Given the diverse applications of LPCs, we have tested both the optimized and calibrated VEHSAs at 3 different temperatures: 223 K, 298 K and 373 K. The optimized device is slightly more resilient to temperature changes due to a reduction of the recombination effects achieved by the optimization of design parameters.

In conclusion, the PhPO method provides optimum design parameters for state-of-the-art and new generation VEHSA devices, opening a new route towards ultra-efficient VEHSAs with application to LPC and tandem solar cells, not necessarily based on direct bandgap materials.

REFERENCES

[1] K. Jin and W. Zhou, "Wireless laser power transmission: A review of recent progress," *IEEE Trans. Power Electron.*, vol. 34, no. 4, pp. 3842–3859, Apr. 2019, doi: 10.1109/TPEL.2018.2853156.

[2] D. Krut, R. Sudharsanan, W. Nishikawa, T. Isshiki, J. Ermer, and N. H. Karam, "Monolithic multi-cell GaAs laser power converter with very high current density," in *Proc. Conf. Rec. 29th IEEE Photovoltaic Specialists Conf.*, 2002, pp. 908–911, doi: 10.1109/pvsc.2002.1190727.

[3] C. Algora, I. García, M. Delgado, R. Peña, C. Vázquez, M. Hinojosa, and I. Rey-Stolle, "Beaming power: Photovoltaic laser power converters for power-by-light," *Joule*, no. 2021, pp. 1–29, Dec. 2021, doi: 10.1016/j.joule.2021.11.014.

[4] M. Matsuura, H. Nomoto, H. Mamiya, T. Higuchi, D. Masson, and S. Fafard, "Over 40-W electric power and optical data transmission using an optical fiber," *IEEE Trans. Power Electron.*, vol. 36, no. 4, pp. 4532–4539, Apr. 2021, doi: 10.1109/TPEL.2020.3027551.

[5] H. Helmers, C. Armbruster, M. von Ravenstein, D. Derix, and C. Schöner, "6-W optical power link with integrated optical data transmission," *IEEE Trans. Power Electron.*, vol. 35, no. 8, pp. 7904–7909, Aug. 2020, doi: 10.1109/TPEL.2020.2967475.

[6] D. Shi, L. Zhang, H. Ma, Z. Wang, Y. Wang, and Z. Cui, "Research on wireless power transmission system between satellites," in *Proc. IEEE Wireless Power Transf. Conf. (WPTC)*, May 2016, pp. 1–4, doi: 10.1109/WPT.2016.7498851.

[7] M. Sanders and J. S. Kang, "Utilization of polychromatic laser system for satellite power beaming," in *Proc. IEEE Aerosp. Conf.* , 2020, pp. 1–7, doi: 10.1109/AERO47225.2020.9172561.

[8] N. Kawashima, K. Takeda, H. Matsuoka, Y. Fujii, and M. Yamamoto, "Laser energy transmission for a wireless energy supply to robots," in *Proc. 22nd Int. Symp. Automat. Robot. Construct.*, Ferrara, Italy, Sep. 2005, doi: 10.22260/ISARC2005/0068.

[9] T. Blackwell, "Recent demonstrations of laser power beaming at DFRC and MSFC," in *Proc. AIP Conf. Proc.*, 2005, pp. 73–85, doi: 10.1063/1.1925133.

[10] S. Fafard, F. Proulx, M. C. A. York, L. S. Richard, P. O. Provost, R. Arès, V. Aimez, and D. P. Masson, "High-photovoltage GaAs vertical epitaxial monolithic heterostructures with 20 thin p/n junctions and a conversion efficiency of 60%," *Appl. Phys. Lett.*, vol. 109, no. 13, Sep. 2016, Art. no. 131107, doi: 10.1063/1.4964120.

[11] H. Helmers, E. Lopez, O. Höhn, D. Lackner, J. Schön, M. Schauerte, M. Schachtner, F. Dimroth, and A. W. Bett, "68.9% Efficient GaAs-based photonic power conversion enabled by photon recycling and optical resonance," *Phys. Status Solidi, Rapid Res. Lett.*, vol. 15, no. 7, pp. 1–7, 2021, doi: 10.1002/pssr.202100113.

[12] J. Schubert, E. Oliva, F. Dimroth, W. Guter, R. Loeckenhoff, and A. W. Bett, "High-voltage GaAs photovoltaic laser power converters," *IEEE Trans. Electron Devices*, vol. 56, no. 2, pp. 170–175, Feb. 2009, doi: 10.1109/TED.2008.2010603.

[13] U. Ortabasi and H. Friedman, "Powersphere: A photovoltaic cavity converter for wireless power transmission using high power lasers," in *Proc. IEEE 4th World Conf. Photovoltaic Energy Conf.*, May 2006, pp. 126–129, doi: 10.1109/WCPEC.2006.279380.

[14] J. Mukherjee, S. Jarvis, M. Perren, and S. J. Sweeney, "Efficiency limits of laser power converters for optical power transfer applications," *J. Phys. D, Appl. Phys.*, vol. 46, no. 26, Jul. 2013, Art. no. 264006, doi: 10.1088/0022-3727/46/26/264006.

[15] S. Fafard and D. P. Masson, "Perspective on photovoltaic optical power converters," *J. Appl. Phys.*, vol. 130, no. 16, Oct. 2021, Art. no. 160901, doi: 10.1063/5.0070860.

[16] C. Outes, E. F. Fernández, N. Seoane, F. Almonacid, and A. J. García-Loureiro, "GaAs vertical-tunnel-junction converter for ultra-high laser power transfer," *IEEE Electron Device Lett.*, vol. 42, no. 12, pp. 1882–1885, Dec. 2021, doi: 10.1109/led.2021.3121501.

[17] N. Seoane, E. F. Fernández, F. Almonacid, and A. García-Loureiro, "Ultra-efficient intrinsic-vertical-tunnel-junction structures for next-generation concentrator solar cells," *Prog. Photovolt., Res. Appl.*, vol. 29, no. 2, pp. 231–237, Feb. 2021, doi: 10.1002/pip.3369.

[18] C. Outes, E. F. Fernández, N. Seoane, F. Almonacid, and A. J. García-Loureiro, "Numerical optimisation and recombination effects on the vertical-tunnel-junction (VTJ) GaAs solar cell up to 10,000 suns," *Sol. Energy*, vol. 203, pp. 136–144, Jun. 2020, doi: 10.1016/j.solener.2020.04.029.

[19] E. F. Fernandez, N. Seoane, F. Almonacid, and A. J. Garcia-Loureiro, "Vertical-tunnel-junction (VTJ) solar cell for ultra-high light concentrations (>2000 suns)," *IEEE Electron Device Lett.*, vol. 40, no. 1, pp. 167–170, Dec. 2018, doi: 10.1109/LED.2018.2880240.

[20] J. F. Lozano, N. Seoane, E. Comesaña, F. Almonacid, E. F. Fernández, and A. García-Loureiro, "Laser power converter architectures based on 3C-SiC with efficiencies 80%," *Sol. RRL*, vol. 6, no. 8, Aug. 2022, Art. no. 2101077, doi: 10.1002/solr.202101077.

[21] S. P. Philipps and A. W. Bett, "III-V multi-junction solar cells and concentrating photovoltaic (CPV) systems," *Adv. Opt. Technol.*, vol. 3, nos. 5–6, pp. 469–478, Dec. 2014, doi: 10.1515/aot-2014-0051.

[22] Y. Cui, D. van Dam, S. A. Mann, N. J. J. van Hoof, P. J. van Veldhoven, E. C. Garnett, E. P. A. M. Bakkers, and J. E. M. Haverkort, "Boosting solar cell photovoltage via nanophotonic engineering," *Nano Lett.*, vol. 16, no. 10, pp. 6467–6471, Oct. 2016, doi: 10.1021/acs.nanolett.6b02971.

[23] D. Masson, F. Proulx, and S. Fafard, "Pushing the limits of concentrated photovoltaic solar cell tunnel junctions in novel high-efficiency GaAs phototransducers based on a vertical epitaxial heterostructure architecture," *Prog. Photovolt., Res. Appl.*, vol. 23, no. 12, pp. 1687–1696, Dec. 2015, doi: 10.1002/pip.2709.

[24] M. C. A. York, F. Proulx, D. P. Masson, A. Jaouad, B. Bouzazi, R. Arès, V. Aimez, and S. Fafard, "Thin n/p GaAs junctions for novel high-efficiency phototransducers based on a vertical epitaxial heterostructure architecture," *MRS Adv.*, vol. 1, no. 14, pp. 881–890, 2016, doi: 10.1557/adv.2016.9.

[25] M. C. A. York, A. Mailhot, A. Boucherif, R. Arès, V. Aimez, and S. Fafard, "Challenges and strategies for implementing the vertical epitaxial heterostructure architechture (VEHSA) design for concentrated photovoltaic applications," *Sol. Energy Mater. Sol. Cells*, vol. 181, pp. 46–52, Jul. 2018, doi: 10.1016/j.solmat.2017.11.034.

[26] S. Čičić and S. Tomić, "Genetic algorithm designed high efficiency laser power converters based on the vertical epitaxial heterostructure architecture," *Sol. Energy Mater. Sol. Cells*, vol. 200, Sep. 2019, Art. no. 109878, doi: 10.1016/j.solmat.2019.03.050.

[27] E. F. Fernández, A. García-Loureiro, N. Seoane, and F. Almonacid, "Band-gap material selection for remote high-power laser transmission," *Sol. Energy Mater. Sol. Cells*, vol. 235, Jan. 2022, Art. no. 111483, doi: 10.1016/j.solmat.2021.111483.

[28] M. C. A. York, F. Proulx, D. P. Masson, A. Jaouad, B. Bouzazi, R. Arès, V. Aimez, and S. Fafard, "Enhanced photocarrier extraction mechanisms in ultra-thin photovoltaic GaAs n/p junctions," *Phys., Simul. Photonic Eng. Photovoltaic Devices*, vol. 9743, Mar. 2016, Art. no. 97430Y, doi: 10.1117/12.2212960.

[29] M. H. Tsutagawa and S. Michael, "Triple junction InGaP/GaAS/Ge solar cell optimization: The design parameters for a 36.2% efficient space cell using silvaco ATLAS modeling & simulation," in *Proc. 34th IEEE Photovoltaic Spec. Conf. (PVSC)*, Jun. 2009, pp. 001954–001957, doi: 10.1109/PVSC.2009.5411544.

[30] R. J. Kilway II, "Five-junction solar cell optimization using Silvaco Atlas," Thesis, Naval Postgraduate School, Monterey, CA, USA, Sep. 2017. [Online]. Available: https://archive.org/details/fivejunctionsola1094556146

[31] Silvaco. (2020). *Silvaco software (version 5.30.0.R)*. [Online]. Available: https://www.silvaco.com
[32] M. Ochoa, E. Barrigón, L. Barrutia, I. García, I. Rey-Stolle, and C. Algora, "Limiting factors on the semiconductor structure of III-V multijunction solar cells for ultra-high concentration (1000-5000 suns)," *Prog. Photovolt., Res. Appl.*, vol. 24, no. 10, pp. 1332–1345, Oct. 2016, doi: 10.1002/pip.2791.
[33] G. B. Lush, H. F. Macmillan, B. M. Keyes, D. H. Levi, M. R. Melloch, R. K. Ahrenkiel, and M. S. Lundstrom, "A study of minority carrier lifetime versus doping concentration in n-type GaAs grown by metalorganic chemical vapor deposition," *J. Appl. Phys.*, vol. 72, no. 4, pp. 1436–1442, Aug. 1992, doi: 10.1063/1.351704.
[34] H. C. Casey, D. D. Sell, and K. W. Wecht, "Concentration dependence of the absorption coefficient for n- and p- type GaAs between 1.3 and 1.6 eV," *J. Appl. Phys.*, vol. 46, no. 1, pp. 250–257, Jan. 1975, doi: 10.1063/1.321330.
[35] S. M. Sze and K. K. Ng, *Physics of Semiconductor Devices*. Hoboken, NJ, USA: Wiley, 2006.

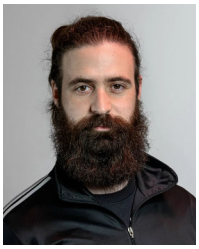

JAVIER F. LOZANO received the M.Res. degree in material physics from the University of Santiago de Compostela, Spain, in 2018, where he is currently pursuing the Ph.D. degree in renewable energies and sustainability.

NATALIA SEOANE received the Ph.D. degree from the University of Santiago de Compostela, Santiago, Spain, in 2007. She was a Visiting Postdoctoral Researcher with the University of Glasgow, Glasgow, U.K., from 2007 to 2009, The University of Edinburgh, Edinburgh, U.K., in 2011, and Swansea University, Swansea, U.K., from 2013 to 2015. She is currently a Postdoctoral Researcher with the University of Santiago de Compostela.

ENRIQUE COMESAÑA (Member, IEEE) received the Ph.D. degree from the University of Santiago de Compostela, Spain, in 2013. He is currently an Assistant Professor with the University of Santiago de Compostela. His research interests include modeling and simulation of electronic devices and application of machine learning techniques to simulations of electrical and electronic systems.

FLORENCIA M. ALMONACID received the M.S. degree in electronic engineering from the University of Granada, Granada, Spain, in 2002, and the Ph.D. degree in electronic engineering from the University of Jaén, Jaén, Spain, in 2009. She is currently a Full Professor with the Department of Electronic and Automatic Engineering, University of Jaén. Her research interests include the application of the artificial neural networks in the field of the photovoltaic technology as well as the characterization and modeling of conventional and concentrator photovoltaic devices and systems.

EDUARDO F. FERNÁNDEZ received the Ph.D. degree in concentrator photovoltaics and multi-junction solar cells from the University of Santiago de Compostela, Spain, in 2012. He is currently the Head of the Advances in Photovoltaic Technology Research Group (AdPVTech; https://adpvtech.com/en/home/), University of Jaén, Spain. He has more than ten years of experience in the field of photovoltaics working in several prestigious institutes, universities, and private companies. He has published over 120 papers indexed in ISI JCR, and presented more than 100 contributions in the most relevant international conferences and workshops. He is also the co-inventor of several patents. He is also a member of more than ten academic and scientific societies.

ANTONIO GARCíA-LOUREIRO (Member, IEEE) received the Ph.D. degree from the University of Santiago de Compostela, Santiago, Spain, in 1999. He is currently a Professor of electronics with the University of Santiago de Compostela. His current research interests include multidimensional simulations of nanoscale transistors and solar cells.